Connectivity Between Primary and Secondary Subglacial Drainage Subsystems Beneath a Land-Terminating Outlet Glacier of the Greenland Ice Sheet

ING, R <http://orcid.org/0000-0001-9767-3209>, BAGSHAW, E <http://orcid.org/0000-0001-8392-1750>, HAWKINS, J, PEACEY, M <http://orcid.org/0000-0001-8554-2797>, DOYLE, S <http://orcid.org/0000-0002-0853-431X>, LIVINGSTONE, S <http://orcid.org/0000-0002-7240-5037>, PRIOR-JONES, M <http://orcid.org/0000-0002-0980-4027>, THORPE, S <http://orcid.org/0009-0003-2034-2606>, MOFFATT, A, SOLE, A <http://orcid.org/0000-0001-5290-8967>, BIANCHI, G <http://orcid.org/0009-0009-6377-6184>, BOOTH, A <http://orcid.org/0000-0002-8166-9608>, BUZZARD, S <http://orcid.org/0000-0003-0722-2549>, CHUDLEY, T <http://orcid.org/0000-0001-8547-1132>, CLASON, C <http://orcid.org/0000-0001-8236-2555>, CRAW, L <http://orcid.org/0000-0002-6809-3587>, EDWARDS, L <http://orcid.org/0000-0001-9936-6966>, GIMBERT, F <http://orcid.org/0000-0001-7350-3563>, HEPBURN, A, JONES, A <http://orcid.org/0000-0001-8662-4049>, LE BRIS, T <http://orcid.org/0009-0009-7424-8686>, MANN, S, MICHEL, A <http://orcid.org/0009-0000-8542-1290>, ROSS, N <http://orcid.org/0000-0002-8338-4905>, STORRAR, Robert <http://orcid.org/0000-0003-4738-0082>, VENESS, Remy <http://orcid.org/0000-0002-2884-3267> and YOUNG, T <http://orcid.org/0000-0001-5865-3459>

ADVANCING EARTH AND SPACE SCIENCES

AGU Advances

RESEARCH ARTICLE

10.1029/2026AV002403

Peer Review The peer review history for this article is available as a PDF in the Supporting Information.

Key Points:

- Hydraulic connectivity between primary and secondary subglacial drainage subsystems switches hourly over spatial scales of hundreds of meters
- Large primary subglacial drainage axes, fed by upstream sources, dictate regional ice dynamics during the melt season
- Wireless "Cryoegg" sensors measure moulin hydraulic head and electrical conductivity and reveal sub-seasonal changes in drainage behavior

Supporting Information:

Supporting Information may be found in the online version of this article.

Correspondence to:

R. Ing,
ryan.ing@ed.ac.uk

Citation:

Ing, R., Bagshaw, E., Hawkins, J., Peacey, M., Doyle, S., Livingstone, S., et al. (2026). Connectivity between primary and secondary subglacial drainage subsystems beneath a land-terminating outlet glacier of the Greenland Ice Sheet. *AGU Advances*, *7*, e2026AV002403. https://doi.org/10.1029/2026AV002403

Received 2 MAR 2026
Accepted 6 AUG 2026

Author Contributions:

Conceptualization: R. Ing, E. Bagshaw, S. Livingstone, M. Prior-Jones, A. Sole, S. Buzzard, R. Storrar
Data curation: R. Ing, J. Hawkins, M. Peacey, S. Doyle, S. Livingstone, M. Prior-Jones, S. Thorpe, S. Buzzard, F. Gimbert, S. Mann, R. Storrar

Connectivity Between Primary and Secondary Subglacial Drainage Subsystems Beneath a Land-Terminating Outlet Glacier of the Greenland Ice Sheet

R. Ing[1,2], E. Bagshaw[2], J. Hawkins[3], M. Peacey[2,4], S. Doyle[4,5], S. Livingstone[5], M. Prior-Jones[3], S. Thorpe[5], A. Moffatt[5], A. Sole[5], G. Bianchi[3], A. Booth[6], S. Buzzard[7], T. Chudley[2,8], C. Clason[8], L. Craw[3], L. Edwards[9], F. Gimbert[10], A. Hepburn[4], A. Jones[11], T. Le Bris[10], S. Mann[3], A. Michel[10], N. Ross[12], R. Storrar[11], R. Veness[11], and T. Young[13]

[1]School of Geosciences, University of Edinburgh, Edinburgh, UK, [2]School of Geographical Sciences, University of Bristol, Bristol, UK, [3]School of Earth & Environmental Sciences, Cardiff University, Cardiff, UK, [4]Department of Geography and Earth Sciences, Centre for Glaciology, Aberystwyth University, Aberystwyth, UK, [5]School of Geography and Planning, University of Sheffield, Sheffield, UK, [6]School of Earth, Environment and Sustainability, University of Leeds, Leeds, UK, [7]Department of Geography and Environmental Sciences, Northumbria University, Newcastle upon Tyne, UK, [8]Department of Geography, Durham University, Durham, UK, [9]School of Biological & Environmental Sciences, Liverpool John Moores University, Liverpool, UK, [10]Institute for Geoscience and Environment IGE, CNRS, Université Grenoble Alps UGA, Grenoble, France, [11]Geography, Environment and Planning, Sheffield Hallam University, Sheffield, UK, [12]School of Geography, Politics and Sociology, Newcastle University, Newcastle upon Tyne, UK, [13]School of Geography and Sustainable Development, University of St Andrews, St Andrews, UK

Abstract The evolution and connectivity of subglacial drainage systems control basal sliding and therefore modulate ice motion, yet direct observations of these systems remain limited. Here, we investigate hydraulic connectivity and its influence on ice motion at Isunnguata Sermia, a large land-terminating outlet glacier of the Greenland Ice Sheet. We use "Cryoegg" wireless sensors to obtain moulin water pressure and electrical conductivity, in conjunction with passive seismics to measure glacio-hydraulic tremor and GNSS-derived measurements of ice motion. We identify rapid switching (<24 hr) of subglacial hydraulic connectivity between distinct subsystems: a large, primary drainage axis located in a deep trough, and secondary subglacial channels. When surface melt inputs are high, the secondary subsystem fed by the instrumented moulins connects with the efficient primary drainage axis and exhibits smoothed diurnal variability and synchronization with regional ice motion and seismic tremor. When surface melt decreases, hydraulic connectivity is reduced, and the secondary subsystem becomes disconnected and responds sensitively to variations in local melt inputs, increasing local meltwater residence time. Regional ice motion is controlled by the characteristics of the primary drainage axis and is insensitive to local inputs into the secondary subsystem.

Plain Language Summary Subglacial drainage systems transport meltwater beneath glaciers to downstream environments. Because the structure of the drainage system controls where water flows and hence how slippery parts of the ice bed may be, it influences ice motion. Yet, directly observing these systems is extremely difficult. We use sensors, including wireless "Cryoeggs" deployed into moulins (quasi-vertical shafts created by surface streams flowing into crevasses), to measure variations in water pressure and electrical conductivity as surface melt fluctuates over the summer melt season. We combine these data with measurements of seismic tremor caused by flowing water, and ice motion from GPS stations to explore the interactions between distinct subsystems: a large primary drainage axis and smaller secondary subglacial channels. We find that variations in surface meltwater input cause the drainage system to rapidly switch between: (a) "connected" states during warm periods, when the distinct subsystems connect and synchronize with regional ice motion; and (b) "disconnected" states associated with cooler periods, when the primary drainage axis becomes more restricted and the system fragments into smaller catchments that respond to local melt inputs. Ice motion is largely controlled by the primary drainage axis rather than the smaller secondary subsystem.

Formal analysis: R. Ing, E. Bagshaw, J. Hawkins, M. Peacey, S. Doyle, S. Livingstone, M. Prior-Jones, A. Sole
Funding acquisition: E. Bagshaw, S. Livingstone, M. Prior-Jones, A. Sole, A. Booth, S. Buzzard, L. Edwards, F. Gimbert, N. Ross, R. Storrar
Investigation: R. Ing, E. Bagshaw, J. Hawkins, M. Peacey, S. Doyle, S. Livingstone, M. Prior-Jones, S. Thorpe, A. Moffatt, A. Sole, G. Bianchi, A. Booth, S. Buzzard, T. Chudley, C. Clason, L. Craw, L. Edwards, F. Gimbert, A. Hepburn, A. Jones, T. Le Bris, S. Mann, A. Michel, N. Ross, R. Storrar, R. Veness, T. Young
Methodology: R. Ing, E. Bagshaw, J. Hawkins, M. Peacey, S. Doyle, S. Livingstone, M. Prior-Jones, S. Thorpe, A. Moffatt, S. Mann, R. Storrar
Project administration: E. Bagshaw, S. Doyle, S. Livingstone, M. Prior-Jones, A. Sole, F. Gimbert, N. Ross, R. Storrar
Resources: E. Bagshaw, J. Hawkins, M. Prior-Jones, F. Gimbert
Software: R. Ing, J. Hawkins, M. Prior-Jones
Supervision: E. Bagshaw, S. Livingstone
Validation: R. Ing, J. Hawkins, S. Doyle, S. Thorpe
Visualization: R. Ing
Writing – original draft: R. Ing, E. Bagshaw, S. Doyle, S. Livingstone, A. Sole
Writing – review & editing: R. Ing, E. Bagshaw, J. Hawkins, M. Peacey, S. Doyle, S. Livingstone, M. Prior-Jones, S. Thorpe, A. Sole, A. Booth, T. Chudley, C. Clason, L. Edwards, F. Gimbert, A. Hepburn, N. Ross, R. Storrar

1. Introduction

Surface meltwater in the ablation area of the Greenland Ice Sheet (GrIS) accesses the glacier bed through crevasses and moulins, and is then routed through the subglacial drainage system. Drainage configurations evolve between hydraulically inefficient, distributed components (e.g., linked cavities, thin films and Darcian flow through permeable sediments; Clarke, 1987; Kamb, 1987) and efficient, channelized structures (Ng, 2000; Nye, 1976; Röthlisberger, 1972) in response to variations in meltwater inputs (Schoof, 2010). The evolving hydraulic connectivity between these configurations determines the overall efficiency of the subglacial drainage system (Lefeuvre et al., 2015; Rada & Schoof, 2018), and controls subglacial water pressure and its transmission across the bed (Lefeuvre et al., 2018; Murray & Clarke, 1995; Werder et al., 2013). Variations in subglacial water pressure modulate basal sliding and ice motion over spatial scales defined by longitudinal stress coupling lengths (Gudmundsson, 2003; Iken & Bindschadler, 1986; Kamb & Echelmeyer, 1986). Measurements of meltwater hydraulic head in moulins or boreholes can thus act as a manometer of these hydrological changes (Andrews et al., 2014; Hubbard et al., 1995).

Direct measurements of subglacial pressure variations are therefore critical for improving our understanding of the subglacial drainage system, its influence on ice sheet dynamics (Andrews et al., 2014; Cowton et al., 2016), and for informing process-based models of subglacial hydrology (Flowers et al., 2003; Hewitt, 2013; M. Hoffman & Price, 2014; Schoof, 2010; Werder et al., 2013). Long-term measurements of water pressure from borehole arrays on mountain glaciers have revealed that subglacial drainage systems can undergo shifts in connectivity. As subglacial water flow declines and water pressure in channels decreases, shifts in local hydraulic gradients can lead to the hydrological isolation of parts of the subglacial system, causing the drainage network to fragment into distinct, isolated subsystems (Rada & Schoof, 2018; Rada Giacaman & Schoof, 2023) that respond independently to local meltwater inputs. Simultaneous measurement of electrical conductivity (EC) can enable proxy assessment of meltwater residence time (Brown et al., 1994), sediment availability (Collins, 1979), and meltwater origin (Gordon et al., 1998), providing further evidence of meltwater isolation.

On the GrIS, direct observations from boreholes have provided detailed records of basal water pressure and assessment of drainage configurations (Andrews et al., 2014; Doyle et al., 2018, 2022; Lüthi et al., 2002; Meierbachtol et al., 2013; Wright et al., 2016). These data are particularly powerful when used alongside surface measurements of ice motion across spatial scales sufficient to capture both regional and local subglacial processes (Andrews et al., 2014; Doyle et al., 2013; Mejia et al., 2022). GNSS-derived ice motion is a well-established method for inferring subglacial drainage efficiency; increases in surface velocity typically relate to regional basal water pressure variations, while surface uplift can indicate hydraulic jacking (Bartholomew et al., 2010; Iken & Bindschadler, 1986; Iken et al., 1983; van de Wal et al., 2008). Passive seismic observations provide a complementary perspective, where glacio-hydraulic tremor serves as a proxy for temporal variations in regional subglacial discharge, where increased turbulence in subglacial channels correlates with higher seismic power at specific frequencies (Bartholomaus et al., 2015; Gimbert et al., 2016; Mejia et al., 2022). However, our current understanding of GrIS subglacial drainage remains limited by the sparse and spatially restricted nature of direct observations. This makes it challenging to infer large-scale drainage connectivity (Lüthi, 2013), particularly given the limited intersection between surface and sub-surface measurements of active drainage routes.

While boreholes offer stochastic access to the subglacial drainage system, often intercepting poorly connected cavities, moulins provide direct access to channelized drainage and the hydraulic response of subglacial channels to surface melt variability. Combining these data with surface dynamic observations (Andrews et al., 2014; Covington et al., 2020; Cowton et al., 2013, 2016; Mejia et al., 2021, 2022) can reveal hydrological behaviors often analogous to those observed in mountain glaciers, including seasonally evolving subglacial drainage that modulates ice sliding speeds (Andrews et al., 2014; Bartholomew et al., 2010). Previous studies have typically targeted moulins with large supraglacial inputs ($\sim 10^{-1}$ to 10 m^3 s^{-1}; e.g., Andrews et al., 2014; Cowton et al., 2016), but the dynamics of smaller, local, secondary channels and their connectivity to larger, primary subglacial drainage axes remain less well constrained. Here we examine the evolving hydraulic connectivity of primary and secondary subglacial drainage subsystems beneath a land-terminating outlet glacier of the GrIS. We deployed novel wireless "Cryoegg" sensors and a cabled piezometer, to measure water pressure and EC in small moulins. These observations were made in tandem with high-resolution GNSS-derived ice motion, passive surface measurements of seismic tremor as a proxy for subglacial water discharge, and meteorological measurements, to characterize the response of an active sector of the GrIS to changing surface melt inputs.

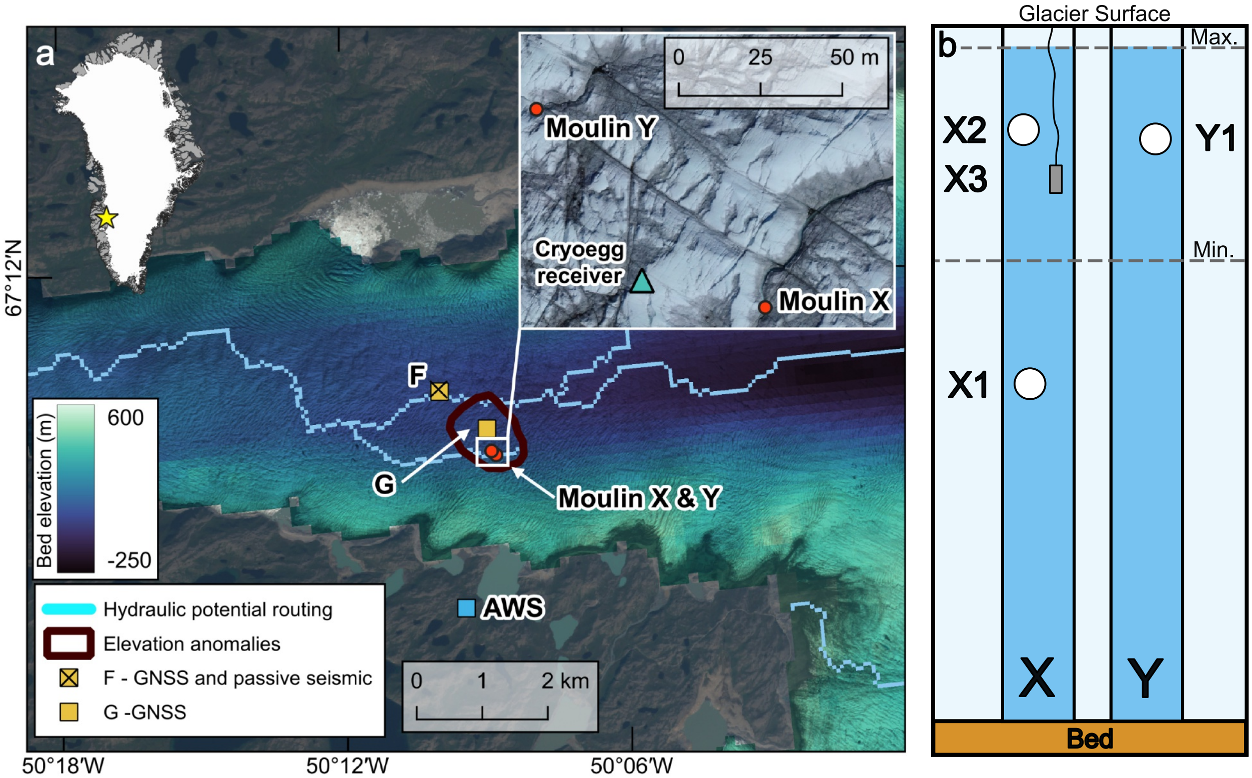

Figure 1. Study site on Isunnguata Sermia in southwest Greenland: (a) Overview of the study area, on a Sentinel-2 true-color image background. The green-blue shading represents the bed elevation from BedMachineV5 (Morlighem et al., 2022). The outline of the elevation anomaly (dark gray polygon) marks the location of a previously drained subglacial lake (Livingstone et al., 2019) and the light blue line shows the subglacial hydraulic potential routing. The inset in the top-right corner shows a UAV true-color orthorectified image of instrumented Moulins X and Y. (b) Schematic cross section of Moulins X and Y with estimated instrument locations (to scale in the vertical dimension), minimum and maximum moulin hydraulic head is denoted by the dashed lines.

2. Methods

2.1. Study Site

Isunnguata Sermia is a large land-terminating outlet glacier on the western margin of the GrIS, situated in an overdeepened subglacial trough ~650 m deep (Lindbäck et al., 2014). Bed topography and subglacial routing from hydraulic potential indicate this trough hosts a major subglacial drainage route (Figure 1a; Livingstone et al., 2019; Pitcher et al., 2020). We define this large-scale feature as the "primary drainage axis," which is fed by the ~14,000 km^2 "regional" catchment up-glacier of our field site (K. D. Mankoff et al., 2020). This primary axis routinely ranks among the four largest annual modeled runoff outlets of the GrIS, with peak summer subglacial discharge estimated on the order of 10^3 m^3 s^{-1} (Figure S5 in Supporting Information S1; K. D. Mankoff et al., 2020).

Our field site is located ~800 m south of this main trough and approximately 8 km from the terminus, in an area where subglacial lake drainages have been previously observed (Livingstone et al., 2019). During July 2024, we instrumented two adjacent moulins (Moulins X and Y, Figure 1a; 67.1753°N 50.1473°W) with active small-scale supraglacial discharge (Figure 1a) and an approximate radius at the surface of 2 m (Figure S1 in Supporting Information S1). We define the subglacial drainage directly beneath these moulins as the "secondary subsystem," which is fed by "local" ice surface catchments of ~30,00 m^2. These local catchment boundaries are difficult to delineate due to the complex surface topography and numerous crevasses, which route meltwater along pathways that shift through the melt season (Figure S2a in Supporting Information S1). Using salt tracing, we determined the typical daily stream discharge into these moulins (and thus the local inputs to the secondary subsystem) during the study period (July to August) to be approximately 0.03–0.06 m^{3}s^{-1} (Table S1 in Supporting Information S1). This is approximately more than four orders of magnitude smaller than the discharge of the primary axis.

2.2. Moulin Instrumentation

Moulin X was instrumented on 12 July 2024 with a Geokon 4500SHSRX vibrating wire piezometer rated to 5 MPa attached to 400 m of cable with an integral high-tensile steel core. The Geokon piezometer was factory calibrated and then zeroed in the field according to the manufacturer's guidance to achieve an accuracy of 0.01 MPa. After calibration, the sensor was gradually lowered into the moulin until the pressure reading stopped increasing when additional cable was released, at which point the cable was anchored at the surface, with 300 m of cable between the sensor and the ice surface. Water pressure and temperature were recorded at 15-min intervals by a Campbell CR1000 logger via a AVW200 vibrating wire interface (Figure S2c in Supporting Information S1).

We also installed two Cryoegg wireless sensors at Moulin X (Prior-Jones et al., 2021), X1 and X2, on the 27 and 17 July 2024 respectively. Moulin Y, located ~90 m northwest from Moulin X, was instrumented with a single Cryoegg (Y1) on the 26 July. The Cryoeggs were deployed by dropping them into a moulin, where they descended via free-fall until becoming lodged or entering the moulin water column (Movie S1). Cryoeggs recorded the water pressure, EC and water temperature and transmitted their data wirelessly via VHF radio to a receiver on the ice surface at hourly intervals (Figure S2a in Supporting Information S1). The Cryoegg pressure and temperature sensor (Keller 7LD, 100 bar) was factory calibrated, whilst the EC sensor was bespoke and calibrated with a dilution series of NaCl solution mixed with surface meltwater, cross-checked with a low-range conductivity meter (Hanna), specifically targeting the most likely range for ice melt (2–50 μS cm^{-1}). Supraglacial meltwater inputs are typically solute-poor with low EC (~0.1–5 μS cm^{-1}; Collins, 1979; Gordon et al., 1998). In contrast, water with subglacial origin can have a substantially higher EC (20–60 μS cm^{-1}; Gordon et al., 1998; Tranter et al., 1997) due to increased contact with subglacial sediments, bedrock and debris-laden ice, and subsequent chemical weathering (Stone & Clarke, 1996). Our sensor was calibrated to maximize sensitivity in these expected ranges. The surface receiver included a barometric pressure sensor (TE Connectivity MS5067-02BA03) to correct water pressure for atmospheric pressure variations, and an Iridium transceiver that transmitted all received data to a UK-based server every hour. The Cryoeggs were modified with a foam and mesh flotation collar, bringing them closer to neutral buoyancy (Figure S2b in Supporting Information S1) to aid their transit through the englacial drainage system.

To estimate sensor depth relative to the bed, we recorded the free-fall of Cryoegg Y1 as it descended through Moulin Y, before it impacted an ice ledge above the moulin's hydraulic head (confirmed by EC readings). We measured the fall duration from the deployment video (Movie S1), as the interval between the frame at which the Cryoegg was released and the frame at which it struck the ledge, identified by an audible thud. We calculated the fall depth from the equation of motion for an object falling under gravity and air drag (Text S1 in Supporting Information S1). We then combined this measurement with ice thickness estimates from nearby ice penetrating radar surveys to find Cryoegg Y1's height above the bed. We assumed hydraulic equilibrium between Moulins X and Y at a reference time during a connected period, identified from the stability of the inter-moulin water-level difference (Figure S3 and Text S1 in Supporting Information S1). Using this reference, we fixed the height of the Moulin X sensors above the bed and converted water depth to orthometric hydraulic head, and water pressure to a percentage of ice overburden (Text S1 in Supporting Information S1). Cryoeggs X2 and Y1, and Geokon X3, were only submerged in water when hydraulic head was high, while Cryoegg X1 provided a full record of moulin hydraulic head.

To calculate the uncertainty in the percentage of ice overburden time series, we used a Monte Carlo analysis that propagated the uncertainties in sensor depth, calibration reference time, and ice thickness (Text S1 and Table S2 in Supporting Information S1). We use one standard deviation of the resulting distribution as our uncertainty, equating to 1.3% for Y1 and 2.2% for the Moulin X sensors. The EC time series from Cryoegg Y1 was anomalous, suggesting the sensor was damaged during deployment. Therefore, the measurements from this sensor are indicative, and only used to detect the transition between submerged and dry conditions.

2.3. Meteorological Data

Hourly surface meltwater production over our field site was modeled using COSIPY—a COupled Snowpack and Ice surface energy and mass-balance model in PYthon (see Sauter et al., 2020), forced by extrapolated data from the PROMICE KAN_L automatic weather station (AWS) (Fausto et al., 2021), which is situated approximately 12 km southeast of our field site at an elevation of ~630 m a.s.l. Air temperature was extrapolated to the elevation of our field site using a lapse rate of −5.3°C km^{-1} (Harper et al., 2011), and atmospheric pressure was corrected using a barometric equation. Precipitation and snowfall data were extracted from the nearest ERA5-Land reanalysis grid cell (native resolution of 9 km, Muñoz-Sabater et al., 2021). While simple extrapolation of variables limits the accuracy of absolute melt values over our field site, the temporal variation in surface melt captures the timing and magnitude of surface water inputs into the subglacial drainage system. We also used air temperature data from an AWS deployed 3 km south of our field site (elevation of 515 m a.s.l.; AWS in Figure 1a). This AWS does not measure all variables needed to force a surface energy balance model, hence the use of KAN_L for calculating surface melt. For investigating rainfall, we also used precipitation data measured by the land-based KAN_B weather station, located 6 km south of our field site.

2.4. Measurements of Horizontal and Vertical Ice Surface Motion

Time series of horizontal and vertical ice surface motion were determined from dual frequency (L1 + L2) Global Navigation Satellite System (GNSS) data recorded by Leica GS10 and GM30 receivers at 0.1 Hz. GNSS stations F (67.1838°N, 50.1661°W) and G (67.1786°N, 50.1495°W) were located 1.2 and 0.3 km from Moulin Y respectively (Figure 1). GNSS antennas were mounted on 6-m-long aluminum poles drilled 5 m into the ice surface. Rapid re-freezing of the hole secured the antenna pole within the ice. Data were post-processed kinematically (King, 2004) relative to a bedrock-mounted reference station using the differential carrier-phase positioning software Track v1.53 (Chen, 1998). Baseline lengths were <4 km and precise ephemerides from the International GNSS Service were used (Dow et al., 2009). Positioning uncertainties were estimated at ~0.01 m in the horizontal and ~0.02 m in the vertical by calculating the standard deviation of the residuals from linear regression applied to the position time series during a month-long period of steady ice motion in November 2023. Small (<5 min) gaps in the position record were linearly interpolated before a second-order 6 hr low-pass Butterworth filter was applied. The position record was then resampled to 10-min medians and differentiated to calculate velocity, which was further filtered using a 6 hr moving average. To prevent phase shifts, phase-preserving filters, differentiation, and resampling methods were used throughout. Vertical displacement due to advection over varying bed topography was removed by calculating local bed slope angles during stable winter periods (Andrews et al., 2014; Hooke et al., 1989). To account for changing topography throughout the season, bed slope values were linearly interpolated between calculations made before and after the 2024 melt season. These calculations assume that basal sliding accounts for 96% of the surface velocity measured by the GNSS receivers (Maier et al., 2019) and that vertical displacement from cavity opening or overburden pressure changes is negligible during non-melt season periods.

2.5. Measurements of Glacio-Hydraulic Seismic Tremor

To characterize water flow in the subglacial drainage system, we installed a seismometer at site F (Figure 1) comprising a C100 Geobit borehole geophone with a corner frequency of 4.5 Hz drilled to 5 m depth and logged by a Digos DATA-CUBE^3 at 100 Hz. Measurements of glacio-hydraulic seismic tremor in alpine glaciers (Gimbert et al., 2016; Nanni et al., 2020) and in Greenland (Bartholomaus et al., 2015; Mejia et al., 2022) have been used as a proxy for subglacial discharge and water pressure. Seismic power was calculated by performing Welch's method over 3 s time windows with 50% overlap (Welch, 1967) on the vertical component of ground motion. This time window was chosen to minimize the influence of short duration but high energy events, such as icequakes. To isolate the seismic tremor caused by subglacial discharge, the mean power between 2 and 10 Hz (Bartholomaus et al., 2015; Gimbert et al., 2016) over 60 s time windows was calculated and displayed in decibels (dB; decimal logarithmic).

3. Results

Between 18 July and 31 August 2024, the subglacial drainage system at our field site exhibited five distinct periods of hydrological behavior. These periods were grouped into two modes defined by the relationship between surface melt, ice velocity, glacio-hydraulic seismic tremor, moulin hydraulic head and moulin EC. During Mode 1, moulin head and ice velocity co-varies (Periods 1, 3 and 5; pale red shading, Figure 2). While in Mode 2, moulin head exhibits large diurnal variations while ice velocity and seismic tremor remain relatively stable or decrease toward background levels (Periods 2 and 4; blue shading, Figure 2).

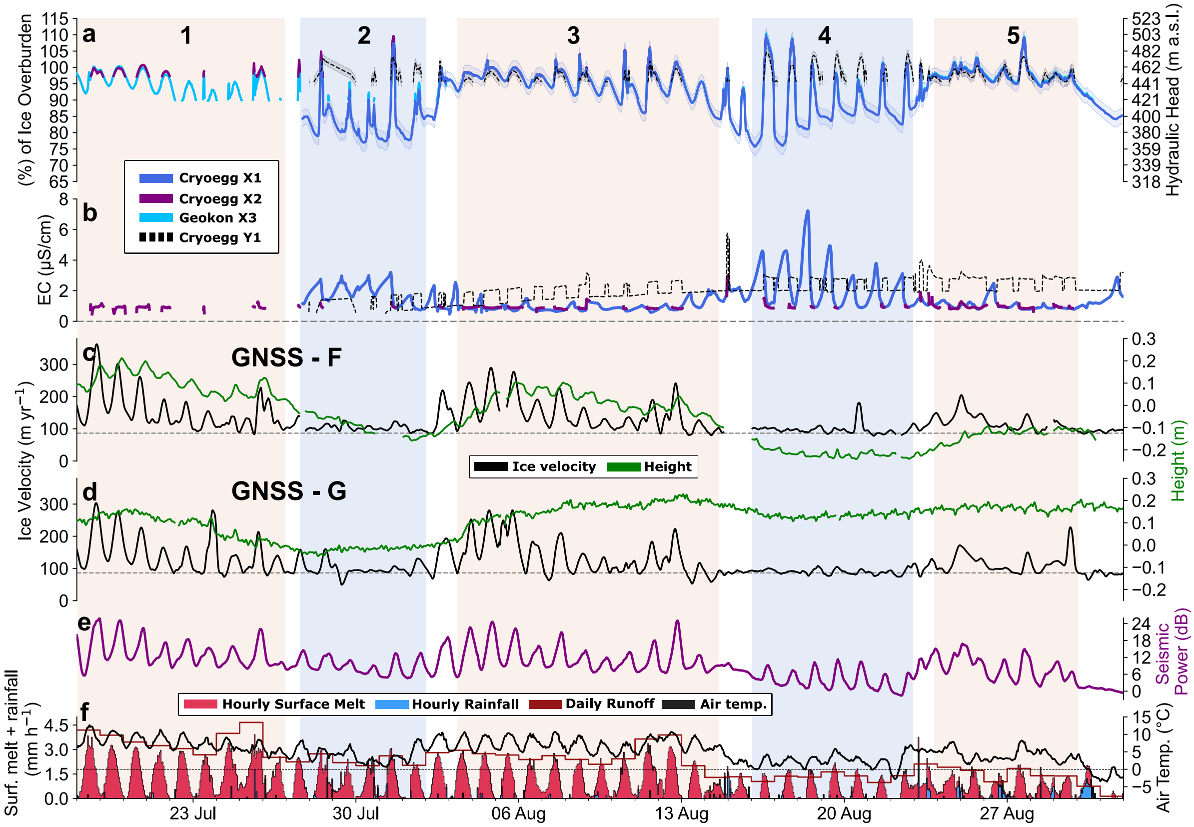

Figure 2. Supra- and englacial measurements from summer 2024. (a) Hydraulic head in Moulin X and Y, with shaded uncertainty bands. (b) Electrical conductivity in Moulin X and Y. (c) GNSS-derived ice velocity (black) and height (green) for GNSS F. (d) Same as (c) for GNSS G. (e) Mean seismic power at F for the frequency range 2–10 Hz. (f) Hourly modeled surface melt (mm w.e. hr^{-1}; red bars), hourly rainfall from KAN_B weather station (mm hr^{-1}; blue bars), daily total runoff (cm w.e. day^{-1}; dark red line), and hourly air temperature at the automatic weather station (black). Bold numbers on (a) denote identified periods discussed in the text. Pale red shading highlights periods of Mode 1 behavior and pale blue periods of Mode 2 behavior. The horizontal dashed gray line on (c) and (d) marks the median winter ice velocity for G. Time is West Greenland Summer Time (UTC -2).

3.1. Period 1 (18–27 July 2024)

Period 1 was characterized by strong diurnal fluctuations of surface melt, ice velocity, seismic tremor and moulin hydraulic head (Figure 2). Peak moulin hydraulic head, ice velocity, surface height and seismic tremor all lagged peak daily surface melt. The mean lag times with respect to melt were 6.7 ± 2.3 hr for hydraulic head, 5.6 ± 1.8 hr for ice velocity at G and F, 10.0 ± 1.6 hr for surface height at F and 8.5 ± 1.3 hr for seismic tremor (Figures 3c–3f). Moulin X hydraulic head averaged ~95% ± 2.2% of ice overburden pressure (~435 m a.s.l. hydraulic head) with smooth diurnal variations of approximately 6% of ice overburden (~25 m hydraulic head) (Figure 2a), while ice velocity exhibited diurnal variations of up to ~200 m yr^{-1} at F and G (Figures 2c and 2d). Between 21 and 24 July, the daily mean moulin hydraulic head decreased, with the water level falling below the Geokon X3 sensor level (equivalent to ~ 89% of ice overburden) for ~10 hr each night between 22 and 27 July (Figure 2a). This reduction in head coincided with declining daily surface melt, a generally decreasing diurnal amplitude of ice velocity from ~200 m yr^{-1} to 50 m yr^{-1} (Figure 2c), and declining seismic tremor at F (Figure 2e). GNSS F, located over a predicted major subglacial drainage route, exhibited diurnal variations in surface height of ~8 cm day^{-1}, and had a background decrease in height of 20 cm (Figure 2c), while GNSS G showed muted diurnal variation but underwent a gradual 21 cm decrease in vertical position (Figure 2d). EC showed no resolvable variation during this period, with values of ~1 μS cm^{-1} (Figure 2b).

3.2. Period 2 (28 July–3 August 2024)

Following two days of elevated surface melt on 24 and 25 July (~4 cm w.e. day^{-1}, Figure 2f), daily melt rates declined and the diurnal melt cycle became less distinct. This reduction in surface melt marked the onset of a shift

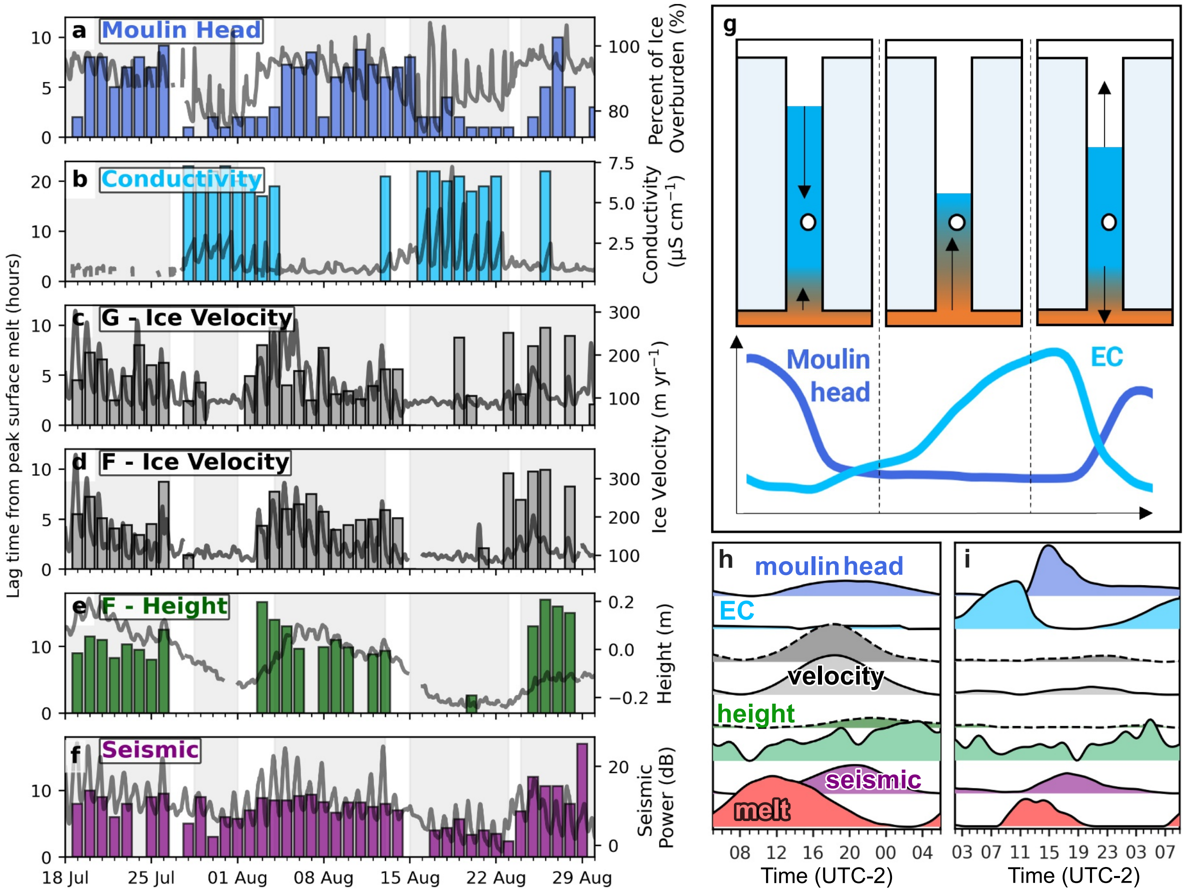

Figure 3. (a–f) Lag times (hours) between daily peaks in surface meltwater production and subsequent peaks in measured variables (bars, left axis). Solid gray lines denote the variation of each variable (right axis). (g) Conceptual model of the diurnal cycle of moulin head and electrical conductivity during a disconnected period (plot shows 17–18 August 2024). (h and i) Stacked normalized waveforms comparing (h) connected (Periods 1, 3, and 5) and (i) disconnected drainage Periods 2 and 4. Line colors for each variable are consistent with plots (a–f). Height and velocity are shown by a solid line for G and dotted line for F.

in dynamic and hydrological behavior, during which ice velocity decoupled from the diurnal surface melt cycle. During Period 2, the lag times for ice velocity and surface height were highly variable or absent due to the muted diurnal variations (Figures 3c–3e). In contrast, the lag time for the moulin hydraulic head decreased to 1.3 ± 0.9 hr, while EC became inversely correlated, peaking 21.5 ± 1.3 hr after peak melt (Figures 3a and 3b). Diurnal variations in head at Moulin X became more pronounced, with an initial rapid increase from 77% to 107% of ice overburden pressure over 6 hr, followed by a decrease to 82% over 3 hr, and then a more gradual decrease overnight to 78% over 14 hr. The maximum diurnal range was ~30% of ice overburden, with pressures reaching a minimum of 77% and occasionally exceeding ice overburden pressure (Figure 2a), notably different to Period 1. This variation in head occurred with no associated increase in height or horizontal ice displacement at G or F, and ice velocities decreased to the winter median or lower (Figures 2c and 2d). Tremor at F exhibited a gradual decline with a smaller diurnal amplitude (Figure 2e) and a reduced lag time, peaking 6.0 ± 2.5 hr after peak surface melt (Figure 3f). EC exhibited a strong, lagged inverse correlation with hydraulic head and melt. For example, EC at Cryoegg X1 (~230 m above the bed) displayed distinct diurnal variations superimposed on a gradual increase over ~17 hr (up to ~2.5 µS cm^{-1}) as moulin hydraulic head decreased and stabilized. This was followed by a rapid decline over ~5 hr as the hydraulic head rose again with the influx of surface meltwater on 31 July (Figure 2a). The daily minimum EC values remained elevated (>1.5 µS cm^{-1}) from 28 to 31 July, with later minimum daily values generally <1 µS cm^{-1}.

3.3. Period 3 (3–14 August 2024)

With increased daily surface melt from the 1 to 2 August (from 2.0 to 2.8 cm w.e. day^{-1}; Figure 2f), the well-coupled behavior observed in Period 1 returned, characterized by large diurnal variations in all variables apart from EC (Figure 2). This re-coupling was also evident in the lag times between peak surface melt and peaks in moulin hydraulic head (6.3 ± 2.2 hr), ice velocity at F and G (5.3 ± 1.8 hr), surface uplift at F (10.7 ± 1.9 hr), and seismic tremor at F (8.2 ± 0.7 hr) (Figures 3a–3f). Moulin X hydraulic head had a mean of ~95% of ice overburden. While the initial diurnal range was ~5%, like Period 1, the variability increased in the latter half of the period to ~15% as surface melt and ice velocity decreased. The almost identical diurnal variations in hydraulic head at Moulin X and Y suggest they were hydraulically well connected (Figure 2a). On several days (e.g., 7–10 August), moulin hydraulic head showed a double-diurnal peak, with an initial spike followed by a secondary sinusoidal curve. Over 4 days from 2 to 6 August, GNSS F and G increased in height, by 26 and 16 cm respectively. Site F showed diurnal variations in surface uplift of 6–8 cm (Figure 2c), while no well-defined diurnal variation was present at G (Figure 2d) and EC remained low (<1 μS cm^{-1}; Figure 2b).

3.4. Period 4 (15–23 August 2024)

Daily surface melt decreased substantially from ~4 cm w.e. day^{-1} on 12 August to ~1.5 cm w.e. day^{-1} by 14 August (Period 4; Figure 2f). This coincided with air temperatures dropping below freezing on 16 August for the first time in the study period (Figure 2f). Ice velocity and surface uplift at G and F were characterized by muted diurnal variability, and their vertical positions decreased by 13 and 23 cm respectively from 13 to 18 August (Figures 2c and 2d). As melt decreased, moulin hydraulic head initially exhibited increased diurnal variability, which subsequently declined throughout the period due to the convergence of maximum and minimum values (Figure 2a). The hydraulic head averaged ~90% of ice overburden during Period 4, with a diurnal range of nearly 33%, and exceeded ice overburden pressure on 17 and 18 August (Figure 2a). The diurnal pattern of hydraulic head resembled Period 2, with a rapid increase followed by a two-step decrease. When submerged, Cryoegg Y1 recorded a similarly high hydraulic head in Moulin Y, with its daily maximum exceeding that of Moulin X by up to 10% of ice overburden pressure (~40 m hydraulic head) from 18 to 23 August (Figure 2a and Figure S4 in Supporting Information S1). EC exhibited a rapid shift in behavior with pronounced diurnal variations of 3 μS cm^{-1} up to a maximum daily value of ~7 μS cm^{-1}, inversely correlated with the hydraulic head (Figure 2b). Moulin hydraulic head had a lag time of only 1.8 ± 1.0 hr, EC of 20.4 ± 1.5 hr and seismic tremor of 3.9 ± 1.0 hr from peak surface melt (Figures 3a–3f).

3.5. Period 5 (24–30 August 2024)

On 24 August, rising air temperature led to increased and more variable overnight surface melt, contrasting with the cessation of melt during the nights of the preceding period (Figure 2f). This shift triggered increased variability in seismic tremor at F (Figure 2e), followed by greater variations in ice velocity at both G and F, alongside a 20 cm rise in surface height at F (Figure 2c). In contrast, the height at G remained relatively stable (Figure 2d). Less pronounced diurnal variability of surface melt rendered the lag times highly variable and difficult to discern (Figures 3a–3f). Between 22 and 26 August, sustained overnight surface melt resulted in a high and stable moulin hydraulic head at both Moulin X and Y, maintaining ~98% of ice overburden pressure with variations of <5% (Figure 2a). Diurnal variations in EC remained muted, stabilizing at around 1 μS cm^{-1} (Figure 2b), except for a 0.5 μS cm^{-1} increase on 26 August, coinciding with a day of low surface melt. After an increase in daily surface melt on 27 August, moulin hydraulic head briefly exceeded ice overburden pressure, followed by an increase in ice velocity at G and F (Figures 2c and 2d). On 30 August, a decline in daily surface melt (Figure 2f) drove a linear decrease in moulin hydraulic head from 98% to 79% of ice overburden pressure over a 2-day period (Figure 2a). This was coincident with a large speed-up event at G (but not F), which was unrelated to surface melt forcing (Figure 2d).

4. Discussion

The behavior exhibited during the five time periods was grouped into two characteristic hydrological modes. The first is "connected" (Mode 1), characterized by regional-catchment dominated drainage within the primary and secondary subsystems, where most variables co-vary (Periods 1, 3 and, to a certain extent, 5). The second is "disconnected" (Mode 2), which indicates more localized controls on drainage within the secondary subsystem

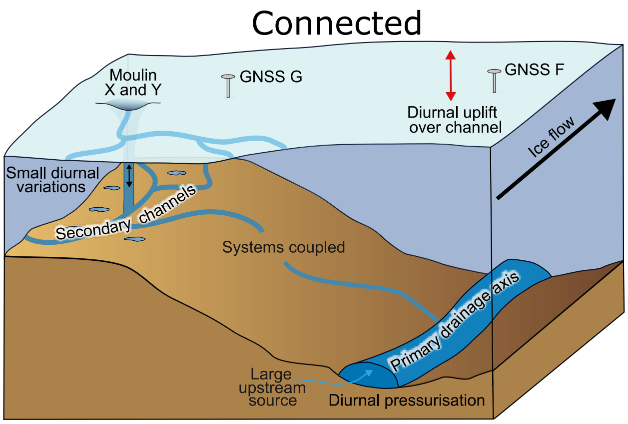

Figure 4. Schematic cross-section of study site for (a) connected periods and (b) disconnected periods showing hypothesized subglacial water movements. Ice flow is obliquely into the page. Figures are not to scale.

(Periods 2 and 4). We attribute the rapid (<24 hr) switching between these modes to interaction between the local secondary subsystem beneath the instrumented moulins and the larger primary drainage axis located within the deep subglacial trough.

4.1. Glaciological Setting of the Instruments

The passive seismic sensor and GNSS at F are located over the ~650-m-deep subglacial trough (Lindbäck et al., 2014), near the primary drainage axis (Figures 1a and 4). We expect the seismic tremor at F (Figure 2e) to represent the hydraulic characteristics of this axis, with high seismic power between 2 and 10 Hz indicating turbulent flow driven by high subglacial discharges and/or hydraulic gradients (Bartholomaus et al., 2015; Gimbert et al., 2016). In contrast, variations in ice velocity (Figures 2c and 2d) are interpreted as a response to changes in basal sliding modulated by average regional basal water pressure (Iken & Bindschadler, 1986; Kamb et al., 1994). The other instruments are located progressively further away from the primary drainage axis. GNSS G is located ~800 m southeast of F, approximately 500 m south of the primary drainage axis. It is situated above the center of a previously drained subglacial lake identified from elevation anomalies in satellite altimetry data (Livingstone et al., 2019; Figure 1a). Moulins X and Y are located 300 m south of GNSS G, approximately 800 m from the primary drainage axis (Figure 4).

Proximity to the primary drainage axis and the lateral extent of its hydraulic influence control the response of the measured variables to changes in surface water inputs. During high melt periods, ice velocity, surface uplift and seismic tremor at F (Figures 2c and 2e) exhibit strong diurnal cycles. This diurnal pattern is related to increasing discharge and daily pressurization in the primary drainage axis as surface meltwater inputs from the regional catchment are routed through the trough. Further away at G (Figure 2d), ice velocity shows a strong response, but the diurnal cycle of surface uplift associated with pressurization of the primary drainage axis is muted (Figure 4). Moulin hydraulic head is episodically in phase with ice velocity (i.e., during "connected" periods), but there are also "disconnected" periods where water pressure exceeds ice overburden pressure with no associated increase in ice velocity or surface uplift at GNSS F or G (e.g., 31 July, 16 and 17 August; Figure 2a). This illustrates the complex response of the ice surface to subglacial hydrological events in a small region: the ice velocity at G and F, along with the seismic tremor at F, reflects regional ice motion controlled by the primary drainage axis near F (Figure 4). In contrast, while hydraulic head in Moulins X and Y (Figure 2a) periodically co-varies with the diurnal ice motion and seismic tremor variations observed at F and G, at other times (e.g., Periods 2 and 4) they respond solely to local surface water inputs. These dynamics suggest that the moulins switch between local (<1 km^2) and regional (>1 km^2, and potentially glacier-scale) responses to melt, depending on their connectivity to the primary drainage axis. This aligns with similar observations from Greenland (Andrews et al., 2014) and beyond (Rada & Schoof, 2018; Rada Giacaman & Schoof, 2023), where the relationship between hydraulic head and ice velocity varies based on drainage connectivity.

4.2. Regional, Connected Subglacial Drainage

The strong diurnal fluctuations in ice motion at F and G during "connected" Periods 1 and 3 (Figures 2c and 2d) are indicative of an efficient, channelized subglacial drainage system, as observed by other studies in the ablation zone of the GrIS (Andrews et al., 2014; Bartholomew et al., 2010; Chandler et al., 2021; Cowton et al., 2016). Diurnal variability in surface melt causes pressurization of the primary drainage axis and surrounding hydraulically connected drainage system (Gordon et al., 1998; Hubbard et al., 1995), reducing basal friction and thus increasing velocity. Transient pressurization of the primary drainage axis explains the strong diurnal surface uplift at F (Figure 2c), a behavior well-documented in other studies (Iken & Bindschadler, 1986; Nienow et al., 2005; Shepherd et al., 2009; Sugiyama et al., 2008). In contrast, surface uplift at G (Figure 2d) does not have a strong diurnal cycle but rather displays a period-dependent cycle comprising increased uplift during Periods 1 and 3 and decreased uplift in Periods 2 and 4 (Figure 2d). Since G is further away from the primary drainage axis (Figures 1 and 4), the effects of pressurization are dampened. This is consistent with Tedstone et al. (2014), who showed that interactions between the channel and the surrounding distributed system help to smooth out local velocity variations caused by pressure fluctuations in the channel.

The large lag times between peak surface melt and ice velocity at F and G (~5 hr, Figure 3) and seismic tremor (~8 hr, Figure 3) suggest that the system is driven by a large, upstream water source (Chandler et al., 2021; Mejia et al., 2022). This behavior aligns with the large scale of the regional Isunnguata Sermia catchment, which ranks among the four largest runoff outlets of the ice sheet (Figure S5 in Supporting Information S1; K. D. Mankoff et al., 2020). In comparison, the nearby Leverett Glacier has a substantially smaller catchment and typically exhibits a smaller lag between surface melt and ice velocity of 2–3 hr (Bartholomew et al., 2011; Shepherd et al., 2009). The ~3 hr difference in lag time between ice velocity and seismic tremor may be because the velocity is associated with the greatest rate of change of melt input (i.e., the steepest part of the rising limb), but tremor peaks at the maximum subglacial discharge.

The moulin hydraulic head variations during Periods 1 and 3 (Figure 2a) align closely with the diurnal behavior recorded by the instruments at F and G (Figures 2c and 2d). Compared with the moulin head variations attributed to efficient, channelized drainage by Andrews et al. (2014), ours have a smaller diurnal range and higher mean. We attribute this difference to the smaller size of our instrumented moulins and the associated channelized secondary subsystem, which exhibits less capacity to accommodate diurnal fluctuations in subglacial discharge. The sinusoidal diurnal cycle in hydraulic head, with a large lag between peak surface melt and hydraulic head (~6 hr, Figure 3a), is interpreted to reflect the smoother regional discharge signal (Chandler et al., 2021; Mejia et al., 2022). This implies that during the "connected" periods, Moulin X (and the secondary subsystem) is hydraulically linked to the primary drainage axis, as locally derived meltwater would typically produce a more immediate response in both water pressure and EC during the efficient mid-melt season, as seen in Periods 2 and 4 (Figures 2a and 2b). However, some days are characterized by two peaks (e.g., 8 August, Figure 2a), with an earlier rapid spike likely representing locally sourced surface meltwater inputs preceding the regional signal. There is an anticlockwise hysteresis between surface melt and ice velocity, seismic tremor, and moulin head (Figure S6 in Supporting Information S1) demonstrating modulation of the system by upstream water (Chandler et al., 2021). The low EC with limited variability suggests an efficient, channelized drainage system with low residence times (Gordon et al., 1998). Consequently, we infer that the EC signal is dominated by supraglacial inputs into the moulin rather than water that has had prolonged contact with the bed (Tranter et al., 1997).

4.3. Local, Disconnected Drainage

Preceding the onset of each disconnected period (Periods 2 and 4), a pronounced increase in daily surface melt (e.g., 25 July and 12 August; Figure 2f) was followed ~2–3 days later by a decrease in surface melt of 50% and 70%, respectively (Figure 2f). We hypothesize that this sequence of events drives the switch to disconnection and the rapid shift in system behavior, characterized by dampened diurnal fluctuations in ice velocity and amplified EC and moulin head. The large increase in daily melt enlarges the primary drainage axis, increasing its capacity. When surface melt subsequently declines, this axis is too large for the reduced discharge and is left underpressurized, which promotes fragmentation of the surrounding connected system (Rada & Schoof, 2018).

The gradual decline in seismic tremor (Figure 2e) with subdued diurnal variations indicates a reduction in discharge and/or water pressure (Nanni et al., 2020), consistent with a subglacial drainage axis that is now largely able to accommodate the reduced melt inputs. The gradual drop in surface height at F and G (Figures 2c and 2d) indicates depressurization of the primary drainage axis and surrounding cavities hydraulically connected to it, leading to increased basal traction and reduced sliding (M. J. Hoffman et al., 2011; Iken & Truffer, 1997; Mair et al., 2001). This behavior is consistent with a decrease in ice velocity to below the winter median (Sole et al., 2013; van de Wal et al., 2008, 2015; Figures 2c and 2d). Because these observations occur in the mid- to late-melt season, when an efficient, channelized drainage network is well-developed, connectivity between the primary and secondary subglacial subsystems is sensitive to the balance between short-term runoff and the existing capacity of the primary drainage axis. The rapid switching between connected and disconnected states is therefore governed by the same short-term fluctuations in meltwater supply that drive variations in regional ice velocity (Bartholomew et al., 2012; Schoof, 2010).

The moulin hydraulic head during Periods 2 and 4 exhibits large diurnal variations, frequently reaching ice overburden pressure, without a corresponding increase in vertical or horizontal ice motion response at G (Figure 2a). This, combined with the reduced lag time (~2 hr; Figure 3a), suggests a direct, local meltwater source. We interpret this behavior to indicate that the secondary subsystem beneath Moulins X and Y becomes hydraulically disconnected from the primary drainage axis or other upstream sources and instead responds to local meltwater inputs.

The high hydraulic head observed during these periods, despite low surface melt and an inferred low-pressure primary drainage axis, reflects the small size of the catchments of the instrumented moulins. When connected, the secondary channels beneath them are kept open by a combination of increased meltwater from the local catchments and discharge from the primary axis; however, once disconnected, the moulins' own meltwater is insufficient to oppose creep closure (Röthlisberger, 1972). Consequently, local pressure rises, at times exceeding ice overburden pressure. This interpretation is further supported by the differences in maximum daily hydraulic head occasionally observed between Moulins X and Y (e.g., 31 July–2 August and 18–23 August; Figure 2a, Figure S4 in Supporting Information S1), despite their proximity (~90 m apart). This difference, of up to ~10% of ice overburden (~40 m; Figure S4 in Supporting Information S1), represents a steep hydraulic gradient that persists only during disconnected periods. Such steep, localized gradients have been observed in other studies and suggest a poorly connected, fragmented subglacial drainage system (Fudge et al., 2008; Murray & Clarke, 1995; Rada Giacaman & Schoof, 2023), indicating that hydraulic connectivity is insufficient to allow pressure equilibration between them. If the moulins are locally isolated, it follows that the secondary channels which they feed are hydraulically isolated from the primary drainage axis. This fragmentation of hydrological features occurs both hydraulically and mechanically due to the increased bridging stress as the primary drainage axis depressurizes (Weertman, 1972). These disconnected periods are similar to the "switching behaviors" observed in previous studies, where subglacial cavities connect to and disconnect from the main channelized system (Andrews et al., 2014; Fudge et al., 2008; Gordon et al., 1998; Murray & Clarke, 1995; Rada & Schoof, 2018).

The larger diurnal fluctuations in EC during Periods 2 and 4 show the influence of meltwater that has had increased contact time with subglacial sediments (Gordon et al., 1998, 2001). Asymmetric moulin hydraulic head (Figure 3i) and longer residence times indicate the transient storage and release of meltwater within the sediments and cavities surrounding the local subglacial channel (Hubbard et al., 1995). As moulin hydraulic head increases during the day, the resulting high pressure forces water into an inefficient distributed system adjacent to the local subglacial channel. When surface melt inputs decrease, hydraulic head drops rapidly. This decline is characterized by two distinct phases: a rapid initial drop in head reduces pressure in both the moulin and the connected subglacial channel while EC remains static and low (Figure 3g); and a subsequent slower decrease overnight as the moulin equilibrates with the pressure of the adjacent distributed system. During this slower decline, the decrease in channel pressure reverses the hydraulic gradient, releasing subglacial water that had been forced into the distributed system earlier in the day (Hubbard et al., 1995; Figure 3g). This process, which can involve Darcian flow through subglacial sediments, returns solute-rich water from the adjacent distributed system into the channel. This water subsequently diffuses up the moulin water column, thereby increasing the EC measured at the sensor location (Gordon et al., 1998).

4.4. Implications for Understanding Ice Sheet Hydrology

The surface topography of the lower ablation area of Isunnguata Sermia is notable for the large number of small (<3 m diameter) moulins (Jones et al., 2018), which generally have small catchments (~30,000 m^2). The transient nature of these surface-to-bed connections, combined with limited surface melt inputs and the high density of moulins, hinders the development of larger hydrological catchments that could support a well-established, extensive channelized subglacial drainage network in this region (Banwell et al., 2016). While large diurnal variations in water pressure occur within these local moulins, they have little impact on ice velocity. Instead, during the melt season, ice velocity is dominated by the influence of the primary drainage axis and the regional background water pressure. This suggests the configuration of the local secondary subsystem has a negligible impact on the spatial pattern of summer ice motion (Tedstone et al., 2014). Consequently, the secondary subsystem acts independently of the primary drainage axis when surface melt and subglacial discharge are low, but it connects to the axis when discharge is high.

We show that connectivity between primary and secondary subsystems beneath the margins of the GrIS changes rapidly and repeatedly, driven by the balance between meltwater supply and the evolving capacity of the primary drainage axis. Despite the location of the instrumented moulins, ~800 m from the primary drainage axis along the subglacial trough (Figure 4), their hydraulic head was frequently influenced by the regional subglacial drainage response. This behavior is consistent with the primary drainage axis becoming overwhelmed and forming connections to the local secondary subsystem (Rada & Schoof, 2018; Rada Giacaman & Schoof, 2023), demonstrating that subglacial channels can have a broad lateral influence on hydrological behavior. The frequent disconnections and large inter-moulin hydraulic gradients we observe demonstrate highly variable connectivity between subsystems. These periods of disconnection could promote temporary storage of subglacial water, a mechanism consistent with the surface expression of subglacial lake drainage previously observed at this location (Lindbäck et al., 2015; Livingstone et al., 2019).

The much larger variations in surface melt and subglacial discharge at this site mean that the lateral scale of connectivity (hundreds of meters) is substantially greater than the <100 m scale estimated from borehole arrays on smaller glaciers (Fudge et al., 2008; Gordon et al., 1998; Hubbard et al., 1995; Rada & Schoof, 2018; Rada Giacaman & Schoof, 2023). These lateral bounds are also consistent with the width of meltwater corridors identified in paleo-ice-sheet settings, supporting the interpretation that these features are the geomorphic expression of hydraulic connectivity (Lewington et al., 2020).

During cooler periods the lateral influence of the primary drainage axis contracts (Figure 4b) as the efficient drainage system that has evolved through the melt season is able to accommodate the smaller, less variable melt inputs, leaving the axis under-pressurized. This promotes fragmentation of the previously channelized drainage surrounding the primary drainage axis into hydraulically disconnected locally influenced subsystems. These processes are unlikely to be unique to this site and probably occur at other outlets with overdeepened beds and small local ice-surface catchments.

Although moulin water pressures frequently exceed ice overburden, they have minimal influence on ice motion, which is controlled by the pressure and extent of the primary drainage axis rather than by local highs in the secondary subsystem. Therefore, moulin records should not be interpreted in isolation, but rather within the context of their connectivity to the primary drainage axis. Our data demonstrate how secondary channels can behave independently; thus, in these settings, moulin records are best viewed as a manometer of local connectivity, providing context for interpreting coincident changes, or lack thereof, in ice velocity (Mejia et al., 2021). Further insights into these hydraulic interactions could also be gained through a dedicated analysis of lag times across different hydrological variables (Mejia et al., 2022). Longer-term records are particularly useful in this context (Rada & Schoof, 2018), especially if supported by other indicators of meltwater residence time such as EC. The use of wireless instruments such as Cryoegg (Prior-Jones et al., 2021) enables the capture of these data with fewer logistical challenges than cabled sensors. Furthermore, integrating these sensors with satellite telemetry enables near-real-time monitoring of drainage system behaviors.

5. Conclusions

Our observations of moulin water pressure, meltwater residence time (inferred from EC), ice motion (horizontal and vertical velocity) and glacio-hydraulic tremor demonstrate the presence of a local secondary subsystem that periodically connects to the wider primary drainage axis. Connectivity between these two subsystems switches rapidly (hourly timescales) and repeatedly (twice during this 6-week record) in response to variations in surface melt input. The repeated disconnection of these subsystems provides evidence of drainage fragmentation in the lower ablation area of the GrIS. When disconnected (Mode 2), local secondary channels become hydraulically isolated (Figure 4b) and experience large water pressure variations, frequently exceeding ice overburden, that have minimal impact on regional ice velocity. Instead, regional ice dynamics are controlled by the pressure of the primary drainage axis and the lateral extent of its hydraulic influence, which stretches at least 800 m (more than one ice thickness) from the trough (Figure 4). This disconnection challenges the assumption that individual moulin or borehole pressure records can act as direct proxies for regional subglacial drainage conditions. While the secondary subsystem has little influence on regional ice motion, observing its behavior and connectivity provides useful context for process-based modeling of subglacial systems.

Global Research Collaboration Statement

The research presented in this study was conducted in Greenland, in the Aasivissuit-Nipisat UNESCO World Heritage Site, over multiple field campaigns. All fieldwork was conducted under relevant science expedition permits issued by the Greenland government (Ministry of Environment and Nature). We are particularly grateful for the logistical and field support provided by Chris Sørensen and the staff at the Kangerlussuaq International Science Support Centre, whose local expertise was vital to the successful and safe completion of our fieldwork.

Conflict of Interest

The authors declare no conflicts of interest relevant to this study.

Availability Statement

The moulin hydraulic head and EC data are available from the Polar Data Centre (Prior-Jones et al., 2026). The modeled surface melt data are available from Ing and Livingstone (2026). The seismological data used are provided by the Epos-France datacenter (Péquegnat et al., 2021) and through the European Integrated Data Archive (EIDA, Strollo et al., 2021). Seismic data will be publicly available under the FDSN network code "9F" by January 2027. Data from the Programme for Monitoring of the Greenland Ice Sheet (PROMICE) are provided by the Geological Survey of Denmark and Greenland (GEUS) at http://www.promice.dk. The PROMICE weather station data sets are available from How et al. (2022). The liquid water discharge data are available at K. Mankoff, (2020). The BedMachine v5 data set is available from Morlighem et al. (2022).

Acknowledgments

The SLIDE team was supported by Natural Environment Research Council (NERC) Grant NE/X000257/1. The GNSS at F was provided by the NERC Geophysical Equipment Facility (loan 1143). RI was supported by a NERC PhD studentship (NE/T00939X/1). MPJ, JDH, LC, SFM and the Cryoegg equipment were supported by a UKRI Future Leaders Fellowship (to MPJ, MR/V022237/1). We acknowledge the support of Kangerlussuaq International Science Support and the local knowledge and guidance of Chris Sørensen. We are grateful to the two anonymous reviewers and the editor for their constructive feedback, which helped improve this manuscript.

References

Andrews, L. C., Catania, G. A., Hoffman, M. J., Gulley, J. D., Lüthi, M. P., Ryser, C., et al. (2014). Direct observations of evolving subglacial drainage beneath the Greenland Ice Sheet. *Nature*, *514*(7520), 80–83. https://doi.org/10.1038/nature13796

Banwell, A., Hewitt, I., Willis, I., & Arnold, N. (2016). Moulin density controls drainage development beneath the Greenland Ice Sheet. *Journal of Geophysical Research: Earth Surface*, *121*(12), 2248–2269. https://doi.org/10.1002/2015JF003801

Bartholomaus, T. C., Amundson, J. M., Walter, J. I., O'Neel, S., West, M. E., & Larsen, C. F. (2015). Subglacial discharge at tidewater glaciers revealed by seismic tremor. *Geophysical Research Letters*, *42*(15), 6391–6398. https://doi.org/10.1002/2015GL064590

Bartholomew, I., Nienow, P., Mair, D., Hubbard, A., King, M. A., & Sole, A. (2010). Seasonal evolution of subglacial drainage and acceleration in a Greenland outlet glacier. *Nature Geoscience*, *3*(6), 408–411. https://doi.org/10.1038/ngeo863

Bartholomew, I., Nienow, P., Sole, A., Mair, D., Cowton, T., & King, M. A. (2012). Short-term variability in Greenland Ice Sheet motion forced by time-varying meltwater drainage: Implications for the relationship between subglacial drainage system behavior and ice velocity. *Journal of Geophysical Research*, *117*(F3). https://doi.org/10.1029/2011JF002220

Bartholomew, I. D., Nienow, P., Sole, A., Mair, D., Cowton, T., King, M. A., & Palmer, S. (2011). Seasonal variations in Greenland Ice Sheet motion: Inland extent and behaviour at higher elevations. *Earth and Planetary Science Letters*, *307*(3), 271–278. https://doi.org/10.1016/j.epsl.2011.04.014

Brown, G. H., Sharp, M. J., Tranter, M., Gurnell, A. M., & Nienow, P. W. (1994). Impact of post-mixing chemical reactions on the major ion chemistry of bulk meltwaters draining the Haut Glacier d'Arolla, Valais, Switzerland. *Hydrological Processes*, *8*(5), 465–480. https://doi.org/10.1002/hyp.3360080509

Chandler, D. M., Wadham, J. L., Nienow, P. W., Doyle, S. H., Tedstone, A. J., Telling, J., et al. (2021). Rapid development and persistence of efficient subglacial drainage under 900 m-thick ice in Greenland. *Earth and Planetary Science Letters*, *566*, 116982. https://doi.org/10.1016/j.epsl.2021.116982

Chen, G. (1998). *GPS kinematic positioning for the airborne laser altimetry at Long Valley, California* (Thesis). Massachusetts Institute of Technology. Retrieved from https://dspace.mit.edu/handle/1721.1/9680

Clarke, G. K. C. (1987). Subglacial till: A physical framework for its properties and processes. *Journal of Geophysical Research*, *92*(B9), 9023–9036. https://doi.org/10.1029/JB092iB09p09023

Collins, D. N. (1979). Quantitative determination of the subglacial hydrology of two Alpine glaciers. *Journal of Glaciology*, *23*(89), 347–362. https://doi.org/10.3189/S0022143000029956

Covington, M. D., Gulley, J. D., Trunz, C., Mejia, J., & Gadd, W. (2020). Moulin volumes regulate subglacial water pressure on the Greenland Ice Sheet. *Geophysical Research Letters*, *47*(20), e2020GL088901. https://doi.org/10.1029/2020GL088901

Cowton, T., Nienow, P., Sole, A., Bartholomew, I., & Mair, D. (2016). Variability in ice motion at a land-terminating Greenlandic outlet glacier: The role of channelized and distributed drainage systems. *Journal of Glaciology*, *62*(233), 451–466. https://doi.org/10.1017/jog.2016.36

Cowton, T., Nienow, P., Sole, A., Wadham, J., Lis, G., Bartholomew, I., et al. (2013). Evolution of drainage system morphology at a land-terminating Greenlandic outlet glacier. *Journal of Geophysical Research: Earth Surface*, *118*(1), 29–41. https://doi.org/10.1029/2012JF002540

Dow, J. M., Neilan, R. E., & Rizos, C. (2009). The international GNSS service in a changing landscape of global navigation satellite systems. *Journal of Geodesy*, *83*(3), 191–198. https://doi.org/10.1007/s00190-008-0300-3

Doyle, S. H., Hubbard, A. L., Dow, C. F., Jones, G. A., Fitzpatrick, A., Gusmeroli, A., et al. (2013). Ice tectonic deformation during the rapid in situ drainage of a supraglacial lake on the Greenland Ice Sheet. *The Cryosphere*, *7*(1), 129–140. https://doi.org/10.5194/tc-7-129-2013

Doyle, S. H., Hubbard, B., Christoffersen, P., Law, R., Hewitt, D. R., Neufeld, J. A., et al. (2022). Water flow through sediments and at the ice-sediment interface beneath Sermeq Kujalleq (Store Glacier), Greenland. *Journal of Glaciology*, *68*(270), 665–684. https://doi.org/10.1017/jog.2021.121

Doyle, S. H., Hubbard, B., Christoffersen, P., Young, T. J., Hofstede, C., Bougamont, M., et al. (2018). Physical conditions of fast glacier flow: 1. Measurements from boreholes drilled to the bed of Store Glacier, West Greenland. *Journal of Geophysical Research: Earth Surface*, *123*(2), 324–348. https://doi.org/10.1002/2017JF004529

Fausto, R. S., van As, D., Mankoff, K. D., Vandecrux, B., Citterio, M., Ahlstrøm, A. P., et al. (2021). Programme for Monitoring of the Greenland Ice Sheet (PROMICE) automatic weather station data. *Earth System Science Data*, *13*(8), 3819–3845. https://doi.org/10.5194/essd-13-3819-2021

Flowers, G. E., Björnsson, H., & Pálsson, F. (2003). New insights into the subglacial and periglacial hydrology of Vatnajökull, Iceland, from a distributed physical model. *Journal of Glaciology*, *49*(165), 257–270. https://doi.org/10.3189/172756503781830827

Fudge, T. J., Humphrey, N. F., Harper, J. T., & Pfeffer, W. T. (2008). Diurnal fluctuations in borehole water levels: Configuration of the drainage system beneath Bench Glacier, Alaska, USA. *Journal of Glaciology*, *54*(185), 297–306. https://doi.org/10.3189/002214308784886072

Gimbert, F., Tsai, V. C., Amundson, J. M., Bartholomaus, T. C., & Walter, J. I. (2016). Subseasonal changes observed in subglacial channel pressure, size, and sediment transport. *Geophysical Research Letters*, *43*(8), 3786–3794. https://doi.org/10.1002/2016GL068337

Gordon, S., Sharp, M., Hubbard, B., Smart, C., Ketterling, B., & Willis, I. (1998). Seasonal reorganization of subglacial drainage inferred from measurements in boreholes. *Hydrological Processes*, *12*(1), 105–133. https://doi.org/10.1002/(SICI)1099-1085(199801)12:1<105::AID-HYP566>3.0.CO;2-

Gordon, S., Sharp, M., Hubbard, B., Willis, I., Smart, C., Copland, L., et al. (2001). Borehole drainage and its implications for the investigation of glacier hydrology: Experiences from Haut Glacier d'Arolla, Switzerland. *Hydrological Processes*, *15*(5), 797–813. https://doi.org/10.1002/hyp.184

Gudmundsson, G. H. (2003). Transmission of basal variability to a glacier surface. *Journal of Geophysical Research*, *108*(B5). https://doi.org/10.1029/2002jb002107

Harper, J., Hubbard, A., Ruskeeniemi, T., Claesson Liljedahl, L., Lehtinen, A., Booth, A., et al. (2011). *The Greenland analogue project*. Yearly report 2010 (Technical Report). Swedish Nuclear Fuel and Waste Management Co.

Hewitt, I. (2013). Seasonal changes in ice sheet motion due to melt water lubrication. *Earth and Planetary Science Letters*, *371*(372), 16–25. https://doi.org/10.1016/j.epsl.2013.04.022

Hoffman, M., & Price, S. (2014). Feedbacks between coupled subglacial hydrology and glacier dynamics. *Journal of Geophysical Research: Earth Surface*, *119*(3), 414–436. https://doi.org/10.1002/2013jf002943

Hoffman, M. J., Catania, G. A., Neumann, T. A., Andrews, L. C., & Rumrill, J. A. (2011). Links between acceleration, melting, and supraglacial lake drainage of the western Greenland Ice Sheet. *Journal of Geophysical Research*, *116*(F4), F04035. https://doi.org/10.1029/2010JF001934

Hooke, R. L., Calla, P., Holmlund, P., Nilsson, M., & Stroeven, A. (1989). A 3 year record of seasonal variations in surface velocity, Storglaciären, Sweden. *Journal of Glaciology*, *35*(120), 235–247. https://doi.org/10.3189/S0022143000004561

How, P., Lund, M. C., Ahlstrøm, A. P., Andersen, S. B., Box, J. E., Citterio, M., et al. (2022). PROMICE and GC-Net automated weather station data in Greenland (Version V39) [Dataset]. *GEUS Dataverse*. https://doi.org/10.22008/FK2/IW73UU

Hubbard, B. P., Sharp, M. J., Willis, I. C., Nielsen, M. K., & Smart, C. C. (1995). Borehole water-level variations and the structure of the subglacial hydrological system of Haut Glacier d'Arolla, Valais, Switzerland. *Journal of Glaciology*, *41*(139), 572–583. https://doi.org/10.3189/S0022143000034894

Iken, A., & Bindschadler, R. A. (1986). Combined measurements of subglacial water pressure and surface velocity of Findelengletscher, Switzerland: Conclusions about drainage system and sliding mechanism. *Journal of Glaciology*, *32*(110), 101–119. https://doi.org/10.3189/S0022143000006936

Iken, A., Röthlisberger, H., Flotron, A., & Haeberli, W. (1983). The uplift of Unteraargletscher at the beginning of the melt season—A consequence of water storage at the bed? *Journal of Glaciology*, *29*(101), 28–47. https://doi.org/10.3189/S0022143000005128

Iken, A., & Truffer, M. (1997). The relationship between subglacial water pressure and velocity of Findelengletscher, Switzerland, during its advance and retreat. *Journal of Glaciology*, *43*(144), 328–338. https://doi.org/10.3189/S0022143000003282

Ing, R., & Livingstone, S. (2026). Daily modelled surface melt of Isunguata Sermia, West Greenland from 2022 to 2024 (Version 1.0) [Dataset]. *NERC EDS UK Polar Data Centre*. https://doi.org/10.5285/0d124098-91a0-4018-a457-f08f0c758ef1

Jones, C., Ryan, J., Holt, T., & Hubbard, A. (2018). Structural glaciology of Isunguata Sermia, West Greenland. *Journal of Maps*, *14*(2), 517–527. https://doi.org/10.1080/17445647.2018.1507952

Kamb, B. (1987). Glacier surge mechanism based on linked cavity configuration of the basal water conduit system. *Journal of Geophysical Research*, *92*(B9), 9083–9100. https://doi.org/10.1029/JB092iB09p09083

Kamb, B., & Echelmeyer, K. A. (1986). Stress-gradient coupling in glacier flow: I. Longitudinal averaging of the influence of ice thickness and surface slope. *Journal of Glaciology*, *32*(111), 267–284. https://doi.org/10.3189/s0022143000015604

Kamb, B., Engelhardt, H., Fahnestock, M. A., Humphrey, N., Meier, M., & Stone, D. (1994). Mechanical and hydrologic basis for the rapid motion of a large tidewater glacier: 2. Interpretation. *Journal of Geophysical Research*, *99*(B8), 15231–15244. https://doi.org/10.1029/94JB00467

King, M. (2004). Rigorous GPS data-processing strategies for glaciological applications. *Journal of Glaciology*, *50*(171), 601–607. https://doi.org/10.3189/172756504781829747

Lefeuvre, P.-M., Jackson, M., Lappegard, G., & Hagen, J. O. (2015). Interannual variability of glacier basal pressure from a 20 year record. *Annals of Glaciology*, *56*(70), 33–44. https://doi.org/10.3189/2015AoG70A019

Lefeuvre, P.-M., Zwinger, T., Jackson, M., Gagliardini, O., Lappegard, G., & Hagen, J. O. (2018). Stress redistribution explains anti-correlated subglacial pressure variations. *Frontiers in Earth Science*, *5*, 110. https://doi.org/10.3389/feart.2017.00110

Lewington, E. L. M., Livingstone, S. J., Clark, C. D., Sole, A. J., & Storrar, R. D. (2020). A model for interaction between conduits and surrounding hydraulically connected distributed drainage based on geomorphological evidence from Keewatin, Canada. *The Cryosphere*, *14*(9), 2949–2976. https://doi.org/10.5194/tc-14-2949-2020

Lindbäck, K., Pettersson, R., Doyle, S. H., Helanow, C., Jansson, P., Kristensen, S. S., et al. (2014). High-resolution ice thickness and bed topography of a land-terminating section of the Greenland Ice Sheet. *Earth System Science Data*, *6*(2), 331–338. https://doi.org/10.5194/essd-6-331-2014

Lindbäck, K., Pettersson, R., Hubbard, A. L., Doyle, S. H., van As, D., Mikkelsen, A. B., & Fitzpatrick, A. A. (2015). Subglacial water drainage, storage, and piracy beneath the Greenland ice sheet. *Geophysical Research Letters*, *42*(18), 7606–7614. https://doi.org/10.1002/2015GL065393

Livingstone, S. J., Sole, A. J., Storrar, R. D., Harrison, D., Ross, N., & Bowling, J. (2019). Brief communication: Subglacial lake drainage beneath Isunguata Sermia, West Greenland: Geomorphic and ice dynamic effects. *The Cryosphere*, *13*(10), 2789–2796. https://doi.org/10.5194/tc-13-2789-2019

Lüthi, M. (2013). Gauging Greenland's subglacial water. *Science*, *341*(6147), 721–722. https://doi.org/10.1126/science.1242672

Lüthi, M., Funk, M., Iken, A., Gogineni, S., & Truffer, M. (2002). Mechanisms of fast flow in Jakobshavn Isbræ, West Greenland: Part III. Measurements of ice deformation, temperature and cross-borehole conductivity in boreholes to the bedrock. *Journal of Glaciology*, *48*(162), 369–385. https://doi.org/10.3189/172756502781831322

Maier, N., Humphrey, N., Harper, J., & Meierbachtol, T. (2019). Sliding dominates slow-flowing margin regions, Greenland Ice Sheet. *Science Advances*, *5*(7), eaaw5406. https://doi.org/10.1126/sciadv.aaw5406

Mair, D., Nienow, P., Willis, I., & Sharp, M. (2001). Spatial patterns of glacier motion during a high-velocity event: Haut Glacier d'Arolla, Switzerland. *Journal of Glaciology*, *47*(156), 9–20. https://doi.org/10.3189/172756501781832412

Mankoff, K. (2020). Streams, Outlets, Basins, and Discharge [k=1.0] [Dataset]. *GEUS Dataverse*. https://doi.org/10.22008/FK2/XKQVL7

Mankoff, K. D., Noël, B., Fettweis, X., Ahlstrøm, A. P., Colgan, W., Kondo, K., et al. (2020). Greenland liquid water discharge from 1958 through 2019. *Earth System Science Data*, *12*(4), 2811–2841. https://doi.org/10.5194/essd-12-2811-2020

Meierbachtol, T., Harper, J., & Humphrey, N. (2013). Basal drainage system response to increasing surface melt on the Greenland Ice Sheet. *Science*, *341*(6147), 777–779. https://doi.org/10.1126/science.1235905

Mejia, J. Z., Gulley, J. D., Trunz, C., Covington, M. D., Bartholomaus, T. C., Breithaupt, C., et al. (2022). Moulin density controls the timing of peak pressurization within the Greenland Ice Sheet's subglacial drainage system. *Geophysical Research Letters*, *49*(22), e2022GL100058. https://doi.org/10.1029/2022GL100058

Mejia, J. Z., Gulley, J. D., Trunz, C., Covington, M. D., Bartholomaus, T. C., Xie, S., & Dixon, T. H. (2021). Isolated cavities dominate Greenland Ice Sheet dynamic response to lake drainage. *Geophysical Research Letters*, *48*(19), e2021GL094762. https://doi.org/10.1029/2021GL094762

Morlighem, M., Williams, C. N., Rignot, E., An, L., Arndt, J. E., Bamber, J. L., et al. (2022). IceBridge BedMachine Greenland, Version 5 [Dataset]. *NASA National Snow and Ice Data Center Distributed Active Archive Center*. https://doi.org/10.5067/GMEVBWFLWA7X

Muñoz-Sabater, J., Dutra, E., Agustí-Panareda, A., Albergel, C., Arduini, G., Balsamo, G., et al. (2021). ERA5-Land: A state-of-the-art global reanalysis dataset for land applications. *Earth System Science Data*, *13*(9), 4349–4383. https://doi.org/10.5194/essd-13-4349-2021

Murray, T., & Clarke, G. K. C. (1995). Black-box modeling of the subglacial water system. *Journal of Geophysical Research*, *100*(B6), 10231–10245. https://doi.org/10.1029/95JB00671

Nanni, U., Gimbert, F., Vincent, C., Gräff, D., Walter, F., Piard, L., & Moreau, L. (2020). Quantification of seasonal and diurnal dynamics of subglacial channels using seismic observations on an Alpine glacier. *The Cryosphere*, *14*(5), 1475–1496. https://doi.org/10.5194/tc-14-1475-2020

Ng, F. (2000). Canals under sediment-based ice sheets. *Annals of Glaciology*, *30*(1), 146–152. https://doi.org/10.3189/172756400781820633

Nienow, P. W., Hubbard, A. L., Hubbard, B. P., Chandler, D. M., Mair, D. W. F., Sharp, M. J., & Willis, I. C. (2005). Hydrological controls on diurnal ice flow variability in valley glaciers. *Journal of Geophysical Research*, *110*(F4), F04002. https://doi.org/10.1029/2003JF000112

Nye, J. F. (1976). Water flow in glaciers: Jökulhlaups, tunnels and veins. *Journal of Glaciology*, *17*(76), 181–207. https://doi.org/10.3189/S002214300001354X

Péquegnat, C., Schaeffer, J., Satriano, C., Pedersen, H., Touvier, J., Saurel, J., et al. (2021). RÉSIF-SI: A distributed information system for French seismological data. *Seismological Research Letters*, *92*(3), 1832–1853. https://doi.org/10.1785/0220200392

Pitcher, L. H., Smith, L. C., Gleason, C. J., Miège, C., Ryan, J. C., Hagedorn, B., et al. (2020). Direct observation of winter meltwater drainage from the Greenland Ice Sheet. *Geophysical Research Letters*, *47*(9), e2019GL086521. https://doi.org/10.1029/2019GL086521

Prior-Jones, M. R., Bagshaw, E. A., Hawkins, J., Craw, L., Mann, S., Peacey, M. W., et al. (2026). Subglacial water pressure, temperature and electrical conductivity measurements from two moulins on Isunnguata Sermia, southwest Greenland (Kalaallit Nunaat), 2024-2025 (Version 1.0) [Dataset]. *NERC EDS UK Polar Data Centre*. https://doi.org/10.5285/c528fbf7-362a-41f7-a060-6b278e67349b

Prior-Jones, M. R., Bagshaw, E. A., Lees, J., Clare, L., Burrow, S., Werder, M. A., et al. (2021). Cryoegg: Development and field trials of a wireless subglacial probe for deep, fast-moving ice. *Journal of Glaciology*, *67*(264), 627–640. https://doi.org/10.1017/jog.2021.16

Rada, C., & Schoof, C. (2018). Channelized, distributed, and disconnected: Subglacial drainage under a valley glacier in the Yukon. *The Cryosphere*, *12*(8), 2609–2636. https://doi.org/10.5194/tc-12-2609-2018

Rada Giacaman, C. A., & Schoof, C. (2023). Channelized, distributed, and disconnected: Spatial structure and temporal evolution of the subglacial drainage under a valley glacier in the Yukon. *The Cryosphere*, *17*(2), 761–787. https://doi.org/10.5194/tc-17-761-2023

Röthlisberger, H. (1972). Water pressure in intra- and subglacial channels. *Journal of Glaciology*, *11*(62), 177–203. https://doi.org/10.3189/S0022143000022188

Sauter, T., Arndt, A., & Schneider, C. (2020). COSIPY v1.3—An open-source coupled snowpack and ice surface energy and mass balance model. *Geoscientific Model Development*, *13*(11), 5645–5662. https://doi.org/10.5194/gmd-13-5645-2020

Schoof, C. (2010). Ice-sheet acceleration driven by melt supply variability. *Nature*, *468*(7325), 803–806. https://doi.org/10.1038/nature09618

Shepherd, A., Hubbard, A., Nienow, P., King, M., McMillan, M., & Joughin, I. (2009). Greenland ice sheet motion coupled with daily melting in late summer. *Geophysical Research Letters*, *36*(1), L01501. https://doi.org/10.1029/2008GL035758

Sole, A., Nienow, P., Bartholomew, I., Mair, D., Cowton, T., Tedstone, A., & King, M. A. (2013). Winter motion mediates dynamic response of the Greenland Ice Sheet to warmer summers. *Geophysical Research Letters*, *40*(15), 3940–3944. https://doi.org/10.1002/grl.50764

Stone, D. B., & Clarke, G. K. C. (1996). In situ measurements of basal water quality and pressure as an indicator of the character of subglacial drainage systems. *Hydrological Processes*, *10*(4), 615–628. https://doi.org/10.1002/(SICI)1099-1085(199604)10:4<615::AID-HYP395>3.0.CO;2-M

Strollo, A., Cambaz, D., Clinton, J., Danecek, P., Evangelidis, C. P., Marmureanu, A., et al. (2021). EIDA: The European integrated data archive and service infrastructure within ORFEUS. *Seismological Research Letters*, *92*(3), 1788–1795. https://doi.org/10.1785/0220200413

Sugiyama, S., Bauder, A., Huss, M., Riesen, P., & Funk, M. (2008). Triggering and drainage mechanisms of the 2004 glacier-dammed lake outburst in Gornergletscher, Switzerland. *Journal of Geophysical Research*, *113*(F4), F04019. https://doi.org/10.1029/2007JF000920

Tedstone, A. J., Nienow, P. W., Gourmelen, N., & Sole, A. J. (2014). Greenland ice sheet annual motion insensitive to spatial variations in subglacial hydraulic structure. *Geophysical Research Letters*, *41*(24), 8910–8917. https://doi.org/10.1002/2014GL062386

Tranter, M., Sharp, M. J., Brown, G. H., Willis, I. C., Hubbard, B. P., Nielsen, M. K., et al. (1997). Variability in the chemical composition of in situ subglacial meltwaters. *Hydrological Processes*, *11*(1), 59–77. https://doi.org/10.1002/(SICI)1099-1085(199701)11:1<59::AID-HYP403>3.0.CO;2-S van de Wal, R. S. W., Boot, W., van den Broeke, M. R., Smeets, C. J. P. P., Reijmer, C. H., Donker, J. J. A., & Oerlemans, J. (2008). Large and rapid melt-induced velocity changes in the ablation zone of the Greenland Ice Sheet. *Science*, *321*(5885), 111–113. https://doi.org/10.1126/science.1158540

van de Wal, R. S. W., Smeets, C. J. P. P., Boot, W., Stoffelen, M., van Kampen, R., Doyle, S. H., et al. (2015). Self-regulation of ice flow varies across the ablation area in south-west Greenland. *The Cryosphere*, *9*(2), 603–611. https://doi.org/10.5194/tc-9-603-2015

Weertman, J. (1972). General theory of water flow at the base of a glacier or ice sheet. *Reviews of Geophysics*, *10*(1), 287–333. https://doi.org/10.1029/RG010i001p00287

Welch, P. (1967). The use of fast Fourier transform for the estimation of power spectra: A method based on time averaging over short, modified periodograms. *IEEE Transactions on Audio and Electroacoustics*, *15*(2), 70–73. https://doi.org/10.1109/TAU.1967.1161901

Werder, M. A., Hewitt, I. J., Schoof, C. G., & Flowers, G. E. (2013). Modeling channelized and distributed subglacial drainage in two dimensions. *Journal of Geophysical Research: Earth Surface*, *118*(4), 2140–2158. https://doi.org/10.1002/jgrf.20146

Wright, P. J., Harper, J. T., Humphrey, N. F., & Meierbachtol, T. W. (2016). Measured basal water pressure variability of the western Greenland Ice Sheet: Implications for hydraulic potential. *Journal of Geophysical Research: Earth Surface*, *121*(6), 1134–1147. https://doi.org/10.1002/2016JF003819

References From the Supporting Information

Porter, C., Howat, I., Noh, M. J., Husby, E., Khuvis, S., Danish, E., et al. (2023). ArcticDEM—Strips, Version 4.1. *Harvard Dataverse, V1*. https://doi.org/10.7910/DVN/3VDC4W

Shreve, R. L. (1972). Movement of water in glaciers. *Journal of Glaciology*, *11*(62), 205–214. https://doi.org/10.3189/S002214300002219X